JTTEE5 13:415-424
DOI: 10.1361/10599630420399
1059-9630/$19.00 © ASM International

Experimental and Numerical Life Prediction of Thermally Cycled Thermal Barrier Coatings

Y. Liu, C. Persson, and J. Wigren

(Submitted October 12, 2002; in revised form July 1, 2003)

This article addresses the predominant degradation modes and life prediction of a plasma-sprayed thermal barrier coating (TBC). The studied TBC system consists of an air-plasma-sprayed bond coat and an air-plasma-sprayed, yttria partially stabilized zirconia top layer on a conventional Hastelloy X substrate. Thermal shock tests of as-sprayed TBC and pre-oxidized TBC specimens were conducted under different burner flame conditions at Volvo Aero Corporation (Trollhättan, Sweden). Finite element models were used to simulate the thermal shock tests. Transient temperature distributions and thermal mismatch stresses in different layers of the coatings during thermal cycling were calculated. The roughness of the interface between the ceramic top coat and the bond coat was modeled through an ideally sinusoidal wavy surface. Bond coat oxidation was simulated through adding an aluminum oxide layer between the ceramic top coat and the bond coat. The calculated stresses indicated that interfacial delamination cracks, initiated in the ceramic top coat at the peak of the asperity of the interface, together with surface cracking, are the main reasons for coating failure. A phenomenological life prediction model for the coating was proposed. This model is accurate within a factor of 3.

Keywords: bond coat oxidation, finite element method, in-plane stress range, life prediction model, stress relaxation, thermal shock tests

1. Introduction

Since the 1980s, thermal barrier coatings (TBCs) have been used as powerful protection for aircraft gas turbine superalloy components against severe temperature environments. Cyclic temperature variation, however, leads to coating failure by delamination and spallation, and thereby exposure of the underlying components to the hot-gas environment. Thus, eventually, the total system might fail. To evaluate the risks associated with any given coating system and to ensure that these coatings are exploited fully, reliable life prediction models are required.

For the development of reliable life prediction models, a thorough understanding of TBC failure mechanisms is a prerequisite. Numerous studies have been conducted experimentally and numerically, resulting in a general agreement that these coatings fail primarily as a result of stresses induced by the thermal expansion mismatch at the ceramic-metal interface, coupled with time-at-temperature processes such as bond coat oxidation, bond coat creep, and creep in the ceramic top coat. However, among the possible mechanisms, dominant life-limiting factors and how they interact are still poorly understood and require further study.

Burner rig tests by Miller and Lowell[1] indicated that stresses due to thermal expansion mismatch on cooling, coupled with the effects of oxidation and plastic deformation of the bond coat, are probable life-limiting factors. DeMasi-Marcin et al.[2] reported that the failure of TBCs is caused by cyclic thermal exposure and occurs by ceramic spallation, which results from the progressive accumulation of ceramic cracking damage parallel and directly adjacent to the rough interface. Cracking damage appears to accumulate by the progressive link-up of multiple small cracks rather than by monotonic propagation of one single dominant crack. Inelastic ceramic deformation, which is attributed to a stick-slip type of behavior in a heavily microcracked, mechanically interlocked, plasma-deposited splat structure, is also reported. Crack initiation is a process of near-threshold growth of pre-existing microcracks instead of direct oxide-induced ceramic crack initiation.[2]

The numerical work of Chang et al.[3] indicated that tensile out-of-plane stresses (i.e., perpendicular to the global average direction of the ceramic-metal interface), in combination with compressive in-plane stresses (i.e., parallel to the global average direction of the interface), resulting from thermal expansion mismatch, favor cracking near the peaks of the asperities of the interface. These cracks do not tend to propagate far into the regions above the valleys between the asperities because this region is under a state of triaxial compression. Oxidation appears to significantly decrease the out-of-plane compression above the valleys and thus may promote further crack extension and eventual coating failure. The study of Freborg et al.[4] demonstrated a strong effect of the bond coat oxidation on ceramic top coat stresses, with influence by other factors, such as bond coat creep, top coat creep, and bond coat roughness. Other studies have declared that the typical stress state in the ceramic top coat adjacent to the interface combines out-of-plane tension and in-plane compression.[5-7] The stresses interact with microdefects to promote crack initiation and growth. When near-interface cracks have grown to a critical size, TBCs fail by spalling, which is usually caused by coating buckling. Most of the previously mentioned studies are concentrated on interfacial crack initiation and

Y. Liu and **C. Persson,** Division of Materials Engineering, Department of Mechanical Engineering, Lund University, SE-22100, Lund, Sweden; and **J. Wigren,** Surface Technology, Volvo Aero Corporation, SE-46181 Trollhüttan, Sweden. Contact e-mail: yan.liu@material.lth.se.

growth. However, Takeuchi and Kokini[8] and Kokini et al.[9] have reported transient thermomechanical loads that favored surface cracking, free-edge cracking as well as interfacial cracking.

Funded by the National Aeronautics and Space Administration (NASA), the Garrett Engine Company, the General Electric Aircraft Engines, and the Pratt & Whitney Aircraft Engine Company have developed different life prediction models dedicated to plasma-sprayed TBCs. The Pratt & Whitney model was thought to be the most extensive one, based on oxide growth at the bond coat on a cycle-by-cycle basis, together with applied cyclic inelastic strain range.[10,11] However, this model did not specifically include the effects of bond coat creep and plasticity, which are thought to be important failure mechanisms for the TBC system.[12-14]

Within the Brite-Euram project 7287, a thermal shock round-robin test was performed by ANSALDO (Ricerche, Italy) BMW-Rolls-Royce Aero Engines, (Germany) and Volvo Aero Corporation (Trollhättan, Sweden) with plasma-sprayed TBC samples that had been thermally cycled until failure.[15] Finite element (FE) models were used to simulate these tests. The transient temperature, stress, and strain distributions during thermal cycling in the coatings were calculated. These models included ceramic top coat creep, bond coat creep, and bond coat plasticity. A wavy sinusoidal interface between the ceramic top coat and the bond coat was introduced into the model. Based on the calculated in-plane stress ranges, a preliminary phenomenological life prediction model of these coatings was developed. However, the model did not incorporate bond coat oxidation. In the current study, both experimental and numerical approaches were applied to evaluate the failure mechanisms of plasma-sprayed TBCs. Through FE modeling, the bond coat oxidation effect was exposed through adding an oxide layer to the interface. The bond coat oxidation was found to significantly change the magnitudes of stress and strain at the interface that refined the developed life prediction models.

2. Experimental Details

2.1 Materials

The studied TBC system consists of an air-plasma-sprayed Ni-23Co-17Cr-12.5Al-0.5Y wt.% bond coat and an air-plasma-sprayed yttria partially stabilized zirconia (ZrO_2-7.5 wt.% Y_2O_3) top coat on a conventional Hastelloy X substrate. The specimens were button-shaped, with a height of 6.7 mm and a diameter of 25.4 mm. The thicknesses of the ceramic top coat and the bond coat were 0.45 and 0.095 mm, respectively.

Twenty-eight specimens, of which 12 were pre-oxidized isothermally in air at 1050 °C for 50 h, were prepared. The pre-oxidation resulted in an alumina layer with approximately 3 μm thickness at the rough wavy interface between the ceramic top coat and the bond coat.

2.2 Thermal Shock Tests

Thermal shock life tests of the two types of TBCs specimens were conducted in a thermal shock test rig, which consisted of a vertical, rotating disc with four heating and four cooling stations, as shown in Fig. 1. Heating on the coating side is obtained using

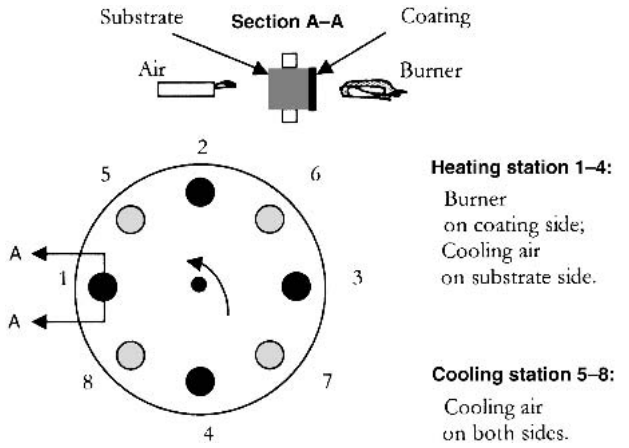

Fig. 1 Schematic of thermal shock test apparatus[6]

four propane/oxygen burner flames. At the same time, cooling is maintained at the substrate backside by a controlled pressurized airflow. Simultaneous cooling at four cooling stations is accomplished by airflow to the backside of the specimens.

The specimens were tack-welded on a plate in such a way that the substrate material could expand and contract freely. This plate was bolted to the rotating disc, which can be rotated at specific angular velocities.

In this study, two different thermal cycles were used. During experiments with shorter cycles, the specimens were heated in the burner flame for 75 s and thereafter were cooled with forced air for another 75 s. In experiments with longer cycles, the specimens were heated and cooled for 180 s, respectively. M210s pyrometers from Mikron were used to measure the temperatures at the coating surface during heating as well as cooling, and on the substrate backside during heating only. The measured temperatures were kept stable until a certain change occurred indicating the start of coating failure.

A video camera system was used for monitoring the coating during testing. The tests were run until coating failure occurred, and the number of cycles to failure was taken as a measure of coating life. Failure was defined to occur when more than 10% of the coating area was spalled off from the ceramic surface. This normally occurred 5-15 cycles before total spalling of the ceramic top coat occurred.

3. FE Analysis

To establish a quantitative understanding of the experimental results, numerical models of the experiments were developed. The FE method was used to calculate the distributions of temperatures, thermal stresses, and thermal strains in the specimens during thermal cycling. These models include a transient thermal analysis followed by a mechanical analysis. Computations were performed using the general purpose FE code ABAQUS[16] on the Lunarc supercomputer at Lund University (Lund, Sweden).

The purpose of this analysis was to study stress distributions in the specimens. The magnitude of these stresses was related to the initiation and growth of cracks. Phenomenological fatigue

life models were developed based on the obtained stress and strain ranges to predict the experimental thermal shock life of the TBCs.

In the thermal analysis, the following assumptions were made: (a) there were no edge effects, due to the large size of the specimens; (b) no oxidation occurred during testing due to the short duration; and (c) a stress-free state occurred at room temperature.

The specimens were modeled as an axisymmetric slice. The FE meshes consisted of 1020 eight-node heat transfer elements or eight-node axisymmetric solid elements. For the as-sprayed specimens, the model consisted of the following three layers: the ceramic top coat; the bond coat; and the superalloy substrate. Pre-oxidized specimens were modeled through the replacement of two rows of bond coat elements with oxide elements (Fig. 2). Thus, an aluminum oxide layer of approximately 3 μm thickness was included at the interface. Surface roughness along the interface was modeled as a sinusoidal wavy face with a wavelength of 110 μm and an amplitude of approximately 25 μm.

In the thermal analysis, transient temperature distributions were calculated by solving the corresponding heat transfer problem. One-dimensional heat transfer in the axial direction of the specimens was assumed. Measured temperatures at the surface of the ceramic top coat and at the backside of the substrate were used to determine boundary conditions, in terms of the heat flux needed for the thermal analysis through comparison of experimentally and numerically obtained temperatures. The obtained temperature distributions were used as input to the mechanical analysis, where corresponding thermal stresses were calculated.

The following boundary conditions were used in the mechanical analysis (Fig. 2): (a) zero radial displacement along symmetry axis OA, (b) constrained displacement along line BC to follow a straight line (simulating a large sample allowed to bend), and (c) fixed point O.

For different material layers, the following assumptions were made: (a) homogenous and isotropic material without macroscopic cracks was used; (b) an elastic-viscoplastic substrate and bond coat were used; (c) a viscoelastic ceramic top coat was used; (d) an elastic alumina layer was used; (e) Norton's creep power law was used for the viscous behavior; and (f) von Mises yield criterion was used for the plastic behavior.

Each material in the models possesses its own temperature-dependent properties and is modeled as a function of temperature over the range from 20-1300 °C. Selected values of these properties at 700 °C are given in Table 1.

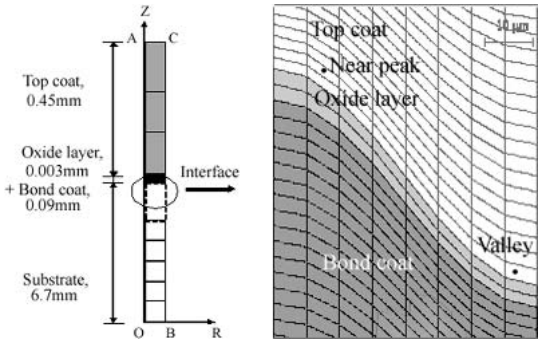

Fig. 2 Schematic of the geometry of the FE model for pre-oxidized TBCs

4. Experimental Results

4.1 Failure Modes

Video recordings of the tests exposed mainly three different failure modes (Fig. 3): (1) chipping, (2) center spallation, and (3) edge spallation. This holds true for as-sprayed specimens as well as for pre-oxidized specimens.

Chipping refers to the spallation of small parts of the ceramic top coats (Fig. 3a). The resulting damage does not reach far down into the ceramic top coats (approximately to a depth of 50 μm). Thus, the capacity of the top coat insulation is not completely lost. Chipping occurs in most tested specimens.

Center spallation is the failure mode in which large parts of the ceramic top coats spall off the specimen (Fig. 3b). In the videos, it can be seen that, before center spallation, delamination of the coatings always occurs, together with cracking on the coating surface. The investigation of failed specimens also indicated that the delamination took place very close to the bond coat. Center spallation has been found in most specimens and was especially pronounced in the pre-oxidized specimens.

Edge spallation refers to the situation in which large parts of the ceramic top coats spall close to the edge of the specimens. At higher temperatures, it was usually found to occur in combination with center spallation.

Microscopic examination of the failed specimens further indicated that spallation of ceramic top coat generally occurs as a

Table 1 Material Properties for Different Layers at 700 °C[10,15,17-19]

Layers	Ceramic Coat	Al_2O_3	Bond Coat	Substrate
E, GPa	17	345	103	150
Poisson's ratio	0.2	0.32	0.27	0.3
Yield stress, MPa	…	…	95	270
CTE(a), $\times 10^{-6}$/°C	11.0	7.79	15	15
Creep behavior(b)	A = 2.50e-21	…	A = 2.04e-34	A = 3.18e-56
	B = 1.59	…	B = 3.35	B = 6.00

(a) CTE, coefficient of thermal expansion
(b) Defined by relationship $\dot{\varepsilon} = A\sigma^B$, where $\dot{\varepsilon}$ is strain rate, A the creep coefficient in units of $MPa^{-B} \cdot s^{-1}$, σ the effective stress in MPa, and B the dimensionless creep exponent.

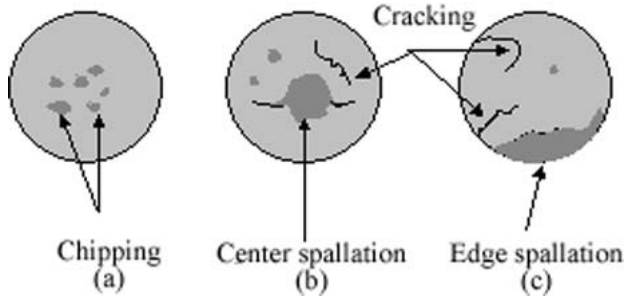

Fig. 3 Schematics of failure modes in thermal shock tests

result of delamination very close to the rough, wavy ceramic-metal interface (at a distance of approximately 5~50 μm), as shown by the arrow in Fig. 4(a). Occasionally, however, horizontal delamination cracking can occur quite far from the interface. The left arrow in Fig. 4(b) shows a horizontal crack approximately 100 μm away from the interface. Even though the horizontal cracking is the main failure mechanism, other kinds of cracking also were found, as shown by the arrows in Fig. 4(b)-(d). The right arrow in Fig. 4(b) indicates that a vertical crack appears to initiate from the surface, whereas the arrow in Fig. 4(c) shows that a vertical crack seems to emerge from a horizontal crack and grow toward the surface. Furthermore, as shown by the arrow in Fig. 4(d), delamination can occur by curving of the horizontal cracks.

The effect of bond coat oxidation on delamination is illustrated in Fig. 5. The arrow in Fig. 5(a) shows an interfacial delamination crack that is connected to the tip of the oxide layer of the bond coat. Such cracks may grow parallel to the interface, touching the oxide layer (Fig. 5a) or may slowly depart from the interface (Fig. 5b).

4.2 Thermal Shock Cycles

Four different temperature cycles were used (Table 2). A typical cycle from test cycle 1 is shown in Fig. 6. Measuring points refer to Fig. 1.

4.3 Thermal Shock Lives

Thermal shock lives measured as the number of cycles to failure, N_f, were determined. Figure 7 shows the mean value of N_f during the four test cycles defined by Table 2. A comparison of values from Table 2 and Fig. 7 shows that the higher the temperature, the shorter the thermal shock life for both the as-sprayed and pre-oxidized specimens. For test cycles 3 and 4, thermal cycling temperatures were almost similar (Table 2), but still the coating life in test cycle 4 was more than twice that in test cycle 3 for the as-sprayed specimens. This indicates that shorter thermal cycles reduced the thermal shock lives of coatings, probably as a result of a more severe heat flux. There is almost no difference in thermal shock lives between as-sprayed and pre-oxidized specimens in test cycles 1 and 2. Only in test cycle 3 did

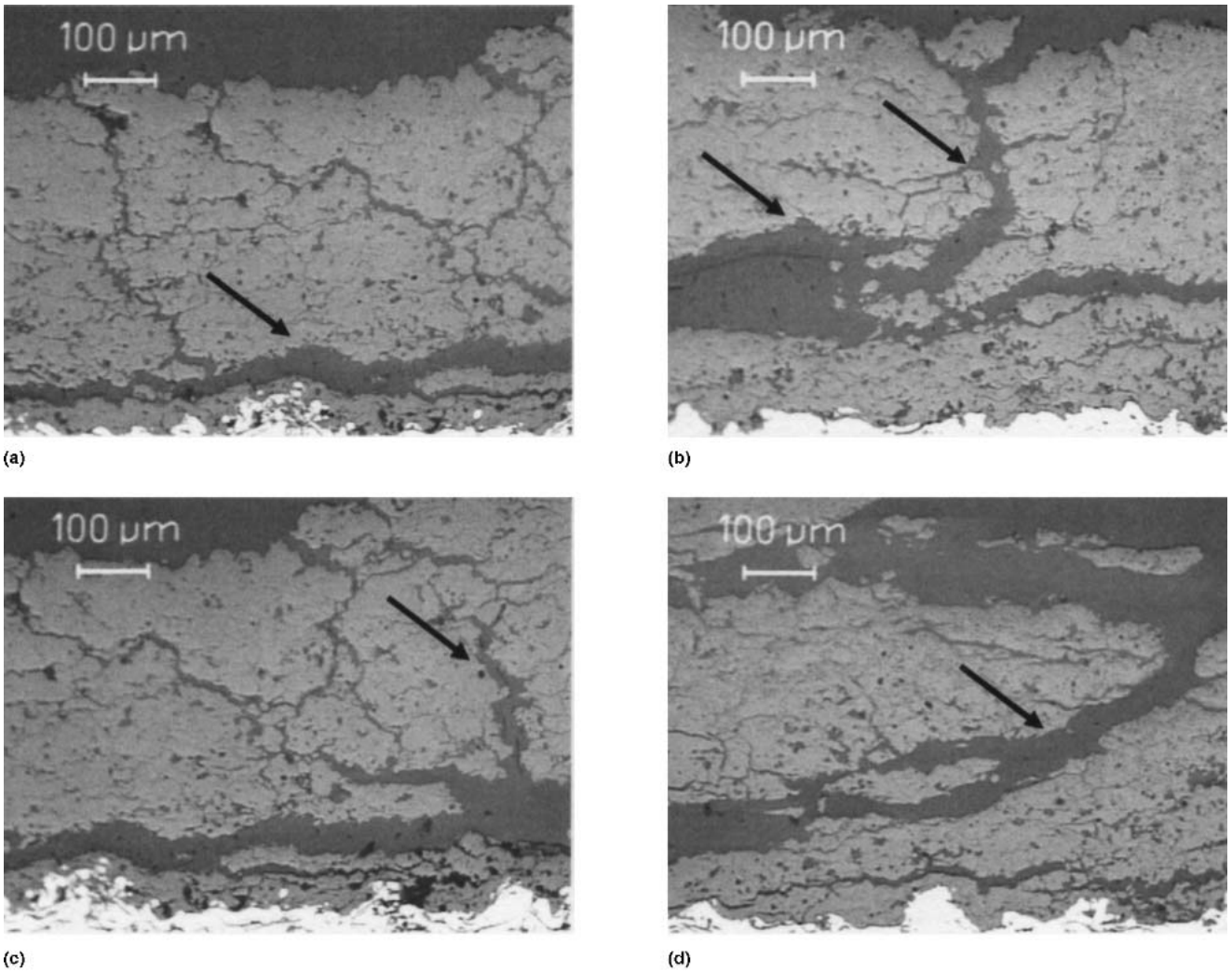

Fig. 4 Optical micrographs of ceramic top coat cracking morphology

the as-sprayed specimens provide a longer thermal shock life than that in the pre-oxidized specimens. It indicates that the effect of a 3 μm thickness oxide layer is important only at high thermal shock temperatures.

5. Numerical Results

5.1 Stress Distribution

The in-plane stresses and the out-of-plane stresses are presented as functions of time and location for different test cycles to depict the stresses that might be the cause of coating failure in a TBC system. From this information, likely failure mechanisms are discussed. In terms of experimental observations, coating cracking was mainly initiated from the interface and/or the top coat surface. Thus, the large amount of data generated during FE modeling will be narrowed to the locations close to the top coat surface, the near-peak position, and the valley regions of the ceramic top coat at the interface, as shown in Fig. 2.

5.2 Stress States of As-Sprayed TBCs

For the cases in which there is no bond coat oxidation in the as-sprayed coatings, stress histories at the three locations in different test cycles are shown in Fig. 8. The stresses during the first four or five cycles are shown.

In test cycle 1, due to a relatively low temperature, only a small amount of creep occurred in the ceramic top coat. Thermal expansion mismatch mainly determines the stress state in the coat. The in-plane stress cycles reached the steady state early (Fig. 8a). It can also be seen that the ceramic of the near-peak

Table 2 Temperatures During Thermal Shock Tests(a)

Test-Cycle No.	T_{max}/T_{min} (Top Coat Surface)(a), °C	T_{max} (Substrate Backside)	Cycling Time Heating/Cooling, s
1	1070/400	860	75/75
2	1230/400	1030	75/75
3	1290/400	1110	75/75
4	1270/400	1000	180/180

(a) T_{max}, maximum temperature; T_{min}, minimum temperature

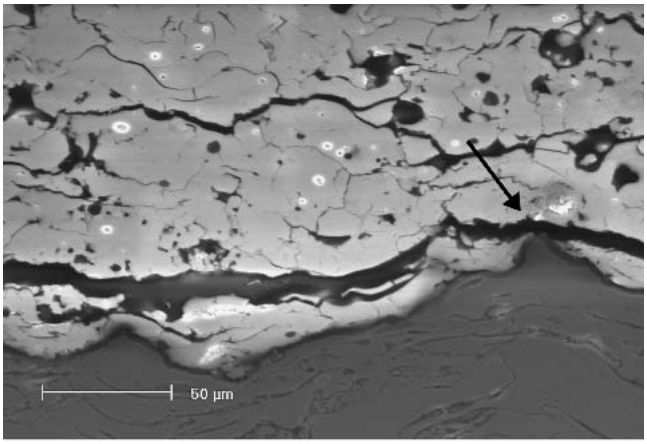

(a)

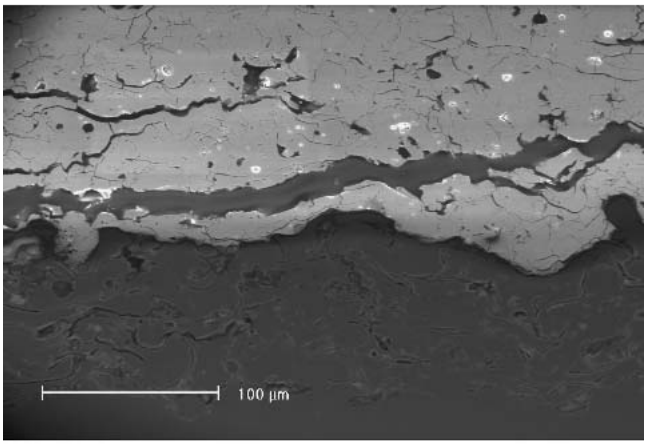

(b)

Fig. 5 Micrographs of cracks at the interface

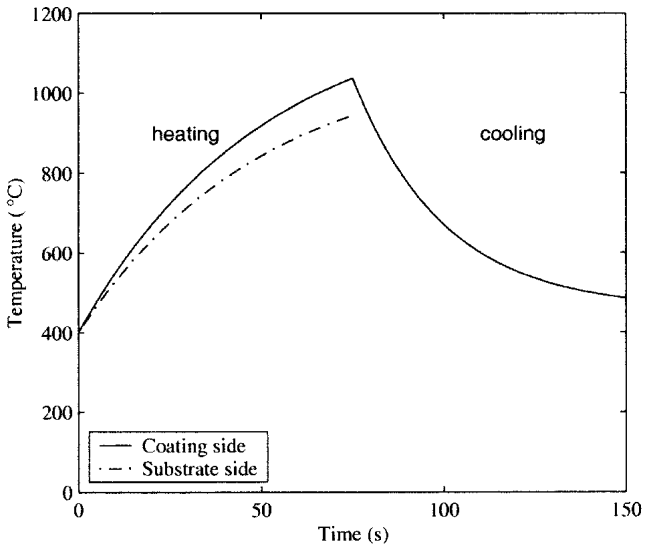

Fig. 6 Measured temperatures during a thermal shock cycle of type 1

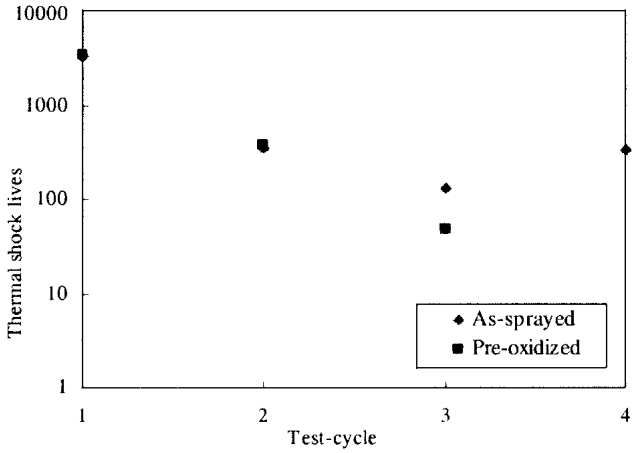

Fig. 7 Thermal shock lives of all the specimens

position was subjected to a tensile stress during the whole cycling process. The stresses at the ceramic top coat surface and in the ceramic valley position cycled between a tensile heat-up stress and a compressive cool-down stress. The out-of-plane stress at the near-peak position of the ceramic top coat changed character after the first two cycles, as shown in Fig. 8(b). It went from being compressive to alternating, probably due to the influence of slight creep and plasticity in the bond coat. The stress concentrations are only located at the coating interface. The out-of-plane stress at the top coat surface was almost zero. The stresses at the near-peak position cycled between a compressive heat-up stress and a tensile cool-down stress, whereas the stresses in the ceramic valley position cycled between a tensile heat-up stress and a compressive cool-down stress.

In test cycle 2, the temperature increased, and the magnitudes of both the tensile in-plane stress and the out-of-plane stress increased during the first few cycles due to more severe thermal expansion mismatches (Fig. 8c and d). However, after the first two or three cycles, the stresses decreased. The possible cause for this was that creep in the ceramic top coat and the bond coat is more pronounced at higher temperatures, which led to stress relaxation. As with any relaxation process, the relaxation rate decreases with time (shown as a decreasing slope of the line generated by connecting the peak heat-up stresses), and the heat-up and cool-down stresses tend toward the steady state. The stress range for heat-up and cool-down portions of the whole cycling process remained constant, with an increasing cycle number at each location. The in-plane stresses at the ceramic near-peak position are driven into tension on heating and turn into compression on cooling. The out-of-plane stress at the ce-

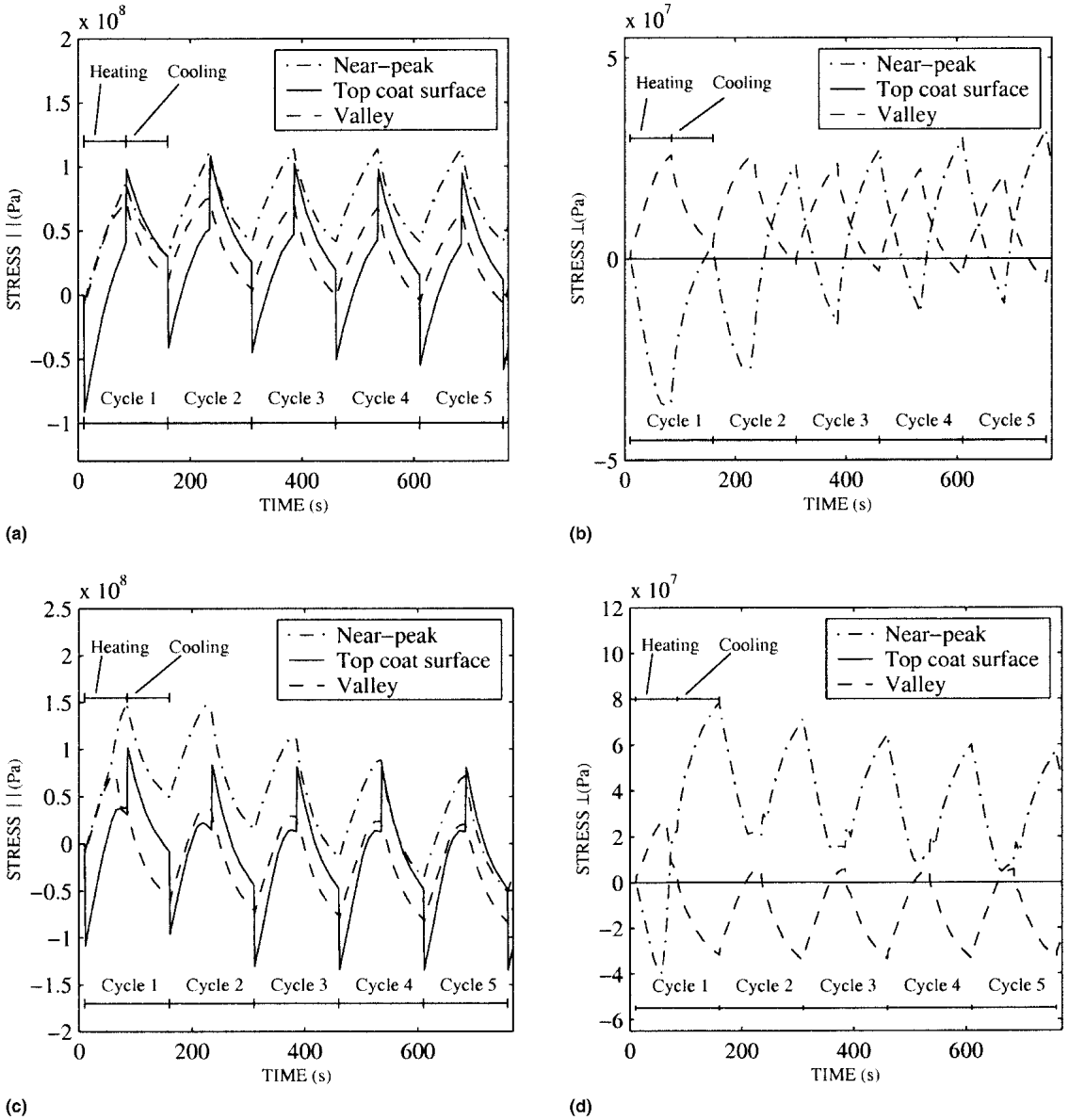

Fig. 8 Histories of **(a)** in-plane and **(b)** out-of-plane stress in test cycle 1; **(c)** in-plane and **(d)** out-of-plane stress in test cycle 2 for as-sprayed TBC systems

ramic near-peak position cycles between slight tension on heating and large tension on cooling, whereas the stress at the ceramic valley position remains approximately compressive during the cycling.

The stress distribution of test cycle 3 was quite similar to that of test cycle 2 because the difference in maximum temperatures between the two cycles was only approximately 60 °C.

Test cycle 4, the longer cycle with higher temperatures, showed almost the same stress levels as test cycle 2. It is even lower than that in test cycle 2, probably due to stress relaxation during the longer heating time in test cycle 4.

5.3 Stress States of Pre-Oxidized TBCs

The introduction of an oxide layer changes the stress levels significantly compared with the non-oxidation cases. The out-of-plane stress especially increased in magnitude, as can be seen from a comparison of Fig. 8 and 9.

For test cycle 1, the oxide layer pushed the near-peak out-of-plane stresses and the valley out-of-plane stresses toward larger tension and compression, respectively (compare Fig. 8b and 9b). The effect of the oxide layer on the in-plane stress was not so significant (compare Fig. 8a and 9a).

With the temperature increase, as in test cycle 2, the oxide layer caused an increase in the near-peak out-of-plane stress during the first cycle. However, the stress decreased very quickly and turned into compression due to creep or stress relaxation (Fig. 8d). The valley out-of-plane stress decreased into a high compression during the first cycle. Then, the compression relaxed as well. Furthermore, the in-plane stress attained a lower level for almost all locations, except for the ceramic top coat

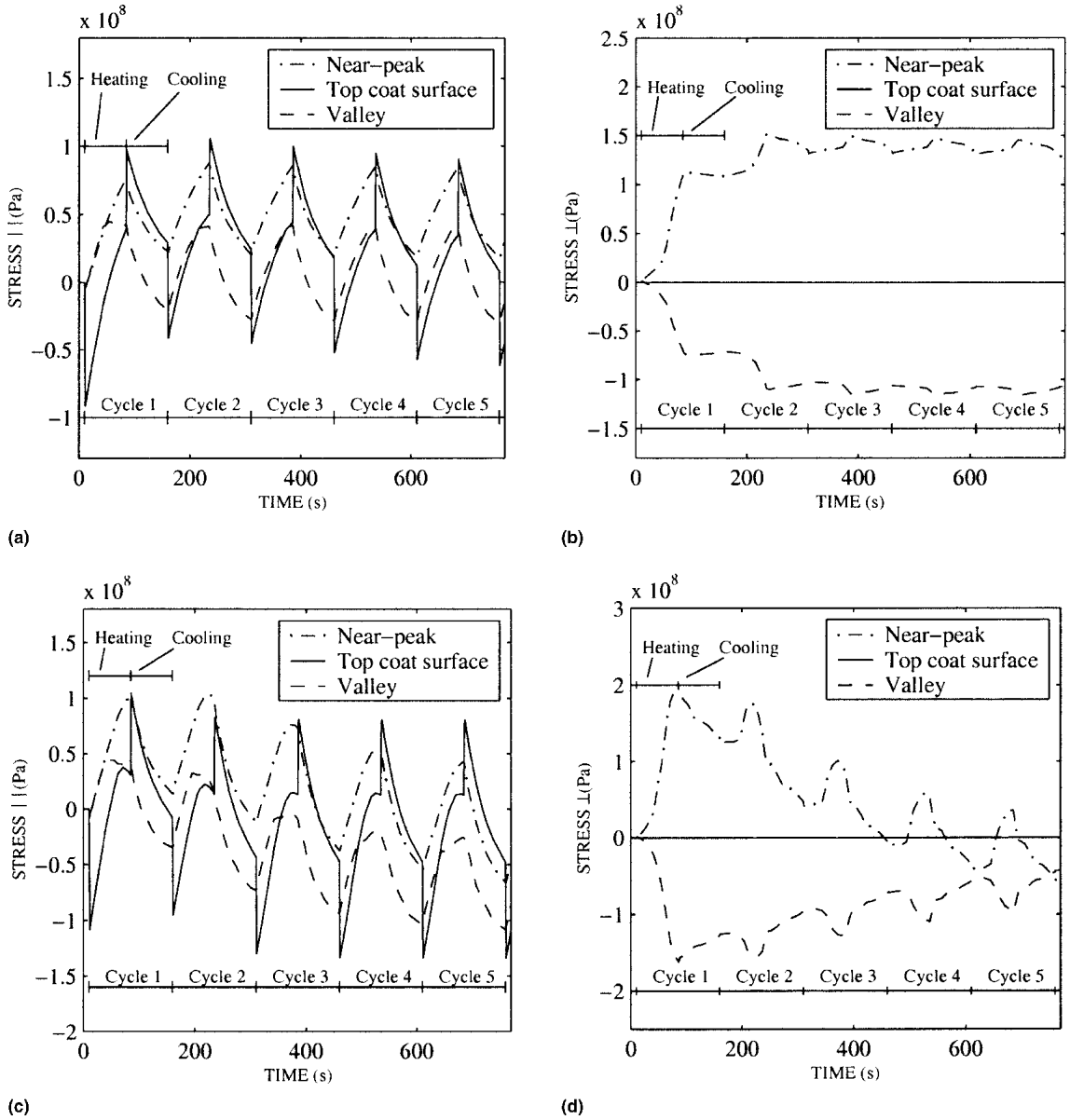

Fig. 9 Histories of **(a)** in-plane and **(b)** out-of-plane stress in test cycle 1; **(c)** in-plane and **(d)** out-of-plane stress in test cycle 2 for pre-oxidized TBC systems

surface (compare Fig. 8c and 9c). Due to the effect of the oxide layer, both the in-plane stress ranges and out-of-plane stress ranges increased slightly for the pre-oxidized cases, as seen in Fig. 8(c) and (d) and Fig. 9(c) and (d).

Along the interface, the out-of-plane stress at the maximum temperature was slightly tensile at the peak position, increased to approximately 50 MPa in the middle position, and decreased to 20 MPa in compression at the valley region (Fig. 10a). As far as the out-of-plane stresses at minimum temperature are concerned, the ceramic top coat was subjected to a compressive stress of more than 100 MPa at the peak position (Fig. 10b). Along the wavy interface, the magnitude of the compressive stress decreased gradually, shifted to a tensile stress of approximately 40 MPa in the middle position, and decreased again to almost zero at the valley.

6. Life Prediction Model

Experiments together with numerical calculations led to the identification of two important coating degradation modes: (a) mechanical degradation, which involves the accumulation of fatigue damage resulting from thermally induced cyclic stresses and strains; and (b) environmental degradation, which involves the effect of the oxide layer on the cyclic stresses and strains.

A generalized fatigue life model for thermal shock conditions of Basquin type is proposed as follows:

$$N_f = A \cdot (\Delta\sigma)^b \quad \text{(Eq 1)}$$

where N_f is the TBC spalling life in cycles, $\Delta\sigma$ is the cyclic stress range, and A and b are constants that are to be fitted to life data collected from the thermal shock tests. This model assumes that the complex loading imposed on the coating system can be adequately presented according to one single parameter.

According to the experimental observation that the coating failed mainly in the ceramic part very close to the interface by thermal fatigue, the coating life should be correlated to the stress range in that region. Since the in-plane stress ranges are larger than the out-of-plane stress ranges, the in-plane stress range was used to fit to Eq 1. The calculated coating lifetime, with the parameters cited above, versus the actual lifetime of the tested coatings is shown in Fig. 11. It was found that the model is able to successfully predict the actual life within three times the scatter bandwidth, which is considered to be adequately accurate.

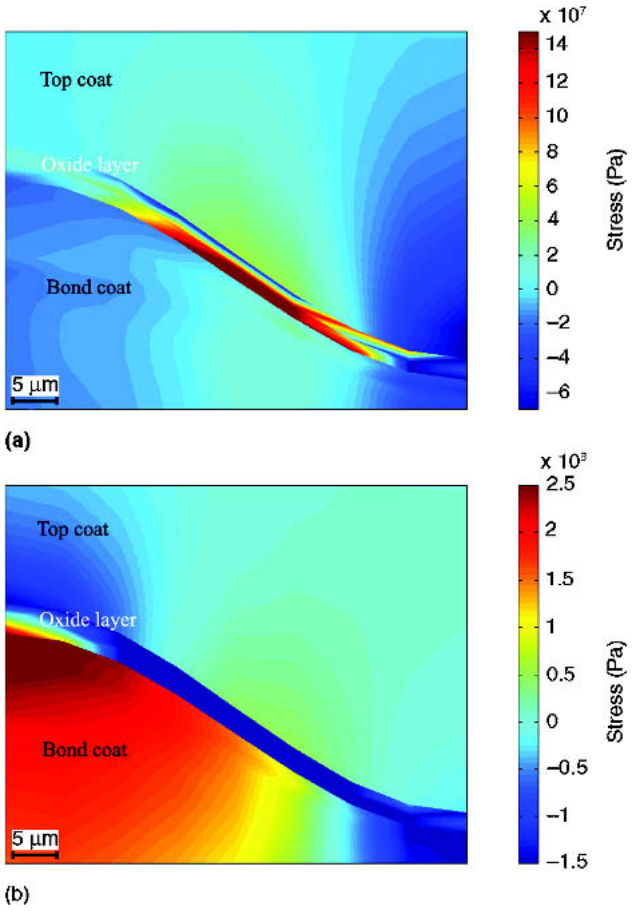

Fig. 10 **(a)** Profile plot of out-of-plane stress after heat-up in a pre-oxidized TBC system following 15 cycles in test cycle 2; and **(b)** profile plot of out-of-plane stress after cool-down in a pre-oxidized TBC system following 15 cycles in test cycle 2

7. Discussion

The results presented above provide insight into the failure mechanisms of thermally cycled TBCs. Among the three failure modes, chipping, center spallation, and edge spallation (Fig. 3), chipping occurs in most coating systems. It is mainly caused by inhomogeneous heating and microdefects in the ceramic top coat. Even though it appears quite frequently, it is not the main

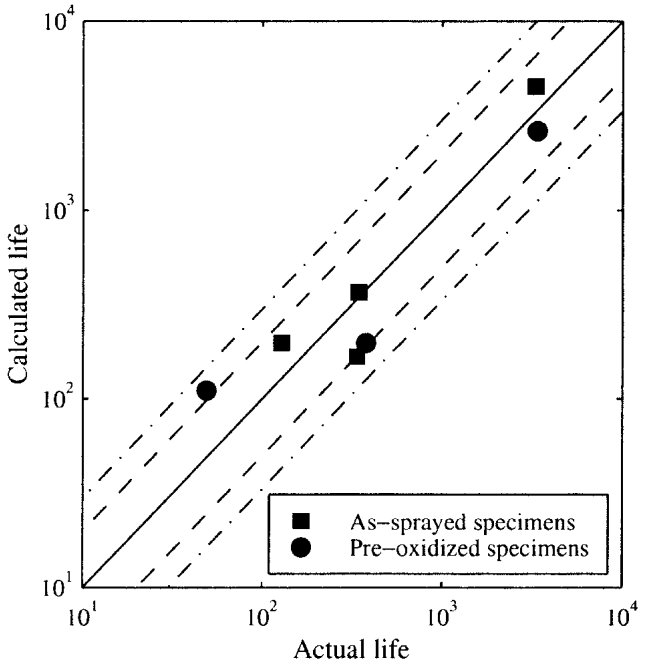

Fig. 11 Calculated coating lives using the in-plane stress range versus actual coating lives obtained in thermal shock tests

fatal failure mechanism because, despite chipping, the ceramic top coat can still work. Therefore, center and edge spallation are the main and critical failure modes related to the stress concentration in the coating.

Usually, spalling is caused by a combination of interfacial delamination and surface cracking. The interfacial delamination is typically initiated by stress concentrations in the interface region, as shown in Fig. 4(a) and 5(a). Delamination cracking also may be caused by microcrack link-up due to the existence of the microdefects in the TBCs. The microcrack link-up may work together with the stress concentrations at the interface. The surface cracking may be initiated by sintering of the ceramic top coat with the help of the stresses that are involved[20,21] in the top coat due to stress relaxation (Fig. 4b and c). Furthermore, a shrinkage vertical crack caused by TBC sintering may reorient into a horizontal delamination.[22]

As mentioned above, the formation of surface cracking and interfacial delamination is dependent on the stress concentration and/or microcrack link-up in the ceramic top coat. The evidence of stress concentrations was provided by the FE analysis. First, recapitulate the as-sprayed TBCs. In the relatively lower thermal cycling temperatures in test cycle 1, both the near-peak in-plane and out-of-plane stresses are tensile after five thermal cycles (Fig. 8a and b). It can be seen in Fig. 8(a) that the in-plane stress reaches a magnitude up to 100 MPa at the near-peak position after heat-up. From the interface to the top coat surface, the in-plane stresses just slightly decrease. Such high in-plane stresses may promote the initiation of vertical cracks near the peak of the asperity and/or surface cracks in the ceramic top coat. Since comparing Fig. 8(a) and (b) shows that the in-plane stress magnitude is larger than the out-of-plane stress magnitude, surface cracking may dominate the crack initiation process.

In test cycle 2, stress relaxation caused by the higher temperature changed the stress state in the coating. The near-peak out-of-plane stress was pushed toward larger tension, whereas the near-peak in-plane tension turned into compression again after cool-down, as shown in Fig. 8(c) and (d). It can also be seen that the maximum in-plane stresses at the top coat surface and the near-peak out-of-plane stresses are almost at the same level. This indicates that both surface cracking and interfacial delamination may be initiated. However, as shown in Fig. 8(d), the out-of-plane stresses vary from peak tension to valley compression along the interface after cool-down. The in-plane stress becomes compressive along the interface region, as shown in Fig. 8(c). The out-of-plane stresses of large tensile magnitude, accompanied by in-plane compressive stresses in the ceramic top coat near the peak of the asperity during the cooling-down stage, may initiate interfacial delamination and propagate it through buckling.

When cycling time increased from 150 s to 6 min, the stress state did not change significantly. This might have been a consequence of stress relaxation.

In the cases in which the bond coat had oxidized, the oxide layer changed the near-peak out-of-plane stress in the ceramic top layer toward 150 MPa when stress relaxation was small, as shown in Fig. 9(b). The in-plane stress in the ceramic top coat did not change significantly compared with that in the no-oxidation case.

As temperature increased in test cycle 2, the near-peak tensile out-plane stresses of a magnitude of 200 MPa built up after heat-up in the first cycle (Fig. 9d). These high stresses could be relieved through such processes as ceramic microcracking, ceramic top coat creep, or bond coat creep. Alternatively, they might initiate interfacial cracking. Through continued cycling, the stresses relax due to the ceramic top coat creep or the bond coat creep, and thus the near-peak tensile out-of-plane stresses decrease quickly and tend toward compression. This indicates that it is the bond coat oxidation but not the stress relaxation that causes the initiation of interfacial cracking.

Furthermore, the complex stress state at the interface also may promote the propagation of interfacial cracking or microcracking in following ways: (a) off-peak tensile out-of-plane stress after cool-down, as shown in Fig. 10(b), might continuously promote cracking; (b) the compressive in-plane stresses due to the stress relaxation after cool-down may cause buckling of interfacial cracks and promote interfacial delamination as in the as-sprayed TBCs (Fig. 8c and 9c); and (c) surface cracks, initiated by sintering with the help of tensile in-plane stress, working together with microcracks, may help to initiate interface cracks.

To simplify the problem, the coating edge spallation, which probably is introduced mainly due to preparation (i.e., grinding edges or overspray) before thermal shock testing, has not been included in the FE models. This may lead to overestimation of the coating life during the modeling.

8. Conclusions

Both thermal shock tests and numerical simulation indicated that the TBC failed by coating delamination followed by spalling. The initiation of cracks followed two paths: (a) interfacial delamination cracking in the ceramic top coating at the peak of the asperity of the interface; and/or (b) surface cracking in the ceramic top coating. Numerical simulations also indicated that bond coat oxidation may lead to interfacial delamination cracking in the ceramic coat very close to the interface, whereas stress relaxation in the ceramic may lead to the buckling of interfacial cracks and promote interfacial delamination.

A phenomenological life prediction model of Basquin type was proposed to predict the coating life. The in-plane stress range that built up in the ceramic top coat close to the interface was found to correlate to the experimentally found coating life. This model is able to successfully predict the actual coating lives with accuracy of a plus or minus a factor of 3.

Acknowledgments

The authors thank Dr. Per Bengtsson, Mr. Sven Olof Stålberg, and Dr. Anne-Céline Leger for all support when performing the thermal shock tests, and Mr. Alexander Evans for help in evaluating the coating lifetime.

References

1. R.A. Miller and C.E. Lowell: "Failure Mechanisms of Thermal Barrier Coatings Exposed to Elevated Temperatures," *Thin Solids Films,* 1982, *95,* pp. 265-73.
2. J.T. DeMasi-Marcin, K.D. Sheffler, and S. Bose: "Mechanisms of Degradation and Failure in a Plasma Deposited Thermal Barrier Coating,"

ASME Paper 89-GT-132, American Society of Mechanical Engineers, 1989.
3. G.C. Chang, W. Phucharoen, and R.A. Miller: "Finite Element Thermal Stress Solutions for Thermal Barrier Coatings," *Surf. Coat. Technol.,* 1987, *32,* pp. 13-28.
4. A.M. Freborg, B.L. Freguson, W.J. Brindley, and G.J. Petrus: "Modeling Oxidation Induced Stresses in Thermal Barrier Coatings," *Mater. Sci. Eng.,* 1998, *A245*(2), pp. 182-90.
5. D.M. Nissley: "Thermal Barrier Coating Life Modeling in Aircraft Gas Turbine Engines," *J. Thermal Spray Technol.,* 1997, *6*(1), pp. 91-98.
6. A.G. Evans, G.B. Crumley, and R.E. Demaray: "On the Mechanical Behavior of Brittle Coatings and Layers," *Oxid. Met.,* 1983, *20*(5/6), pp. 193-216.
7. C.A. Andersson: "Thermal Stress Fracture of Ceramic Coatings," *Fract. Mech. Ceram.,* 1983, *6,* pp. 497-509.
8. Y.R. Takeuchi and K. Kokini: "Thermal Fracture of Multilayer Ceramic Thermal Barrier Coatings," *Trans. ASME,* 1994, *116,* pp. 266-71.
9. K. Kokini, B.D. Choules, and Y.R. Takeuchi: "Thermal Fracture Mechanisms in Ceramic Thermal Barrier Coatings," *J. Thermal Spray Technol.,* 1997, *6*(1), pp. 43-49.
10. J.T. DeMasi, K.D. Sheffler, and M. Ortiz: "Thermal Barrier Coating Life Prediction Model Development: Phase I-Final Report," NASA CR-182230, National Aeronautics and Space Administration, Washington, DC, 1989.
11. R.A. Miller: "Life Modeling of Thermal Barrier Coatings for Aircraft Gas Turbine Engines," *J. Eng. Gas Turbines Power Trans. ASME,* 1989, *111,* pp. 301-05.
12. D.J. Wortman, E.C. Duderstadt, and W.A. Nelson: "Bond Coat Development for Thermal Barrier Coatings," ASME paper 89-GT-134, ASME International, New York, NY, 1999, *3,* pp. 1927-32.
13. W.J. Brindley and R.A. Miller: "Thermal Barrier Coating Life and Isothermal Oxidation of Low-Pressure Plasma-Sprayed Bond Coat Alloys," *Surf. Coat. Technol.,* 1990, *43/44,* pp. 446-57.
14. W.J. Brindley: "Properties of Plasma-Sprayed Bond Coats," *J. Thermal Spray Technol.,* 1997, *6*(1), pp. 85-90.
15. Y. Liu, C. Persson, C. Gualco, T. Haubold, D. Schwingel, R. Taylor, and J. Wigren: "Life Prediction of Thermally Cycled Thermal Barrier Coatings" in *Proceedings of the Seventh International Fatigue Congress,* X.R. Wu and Z.G. Wang, ed., 1999, *3,* pp. 1927-32.
16. ABAQUS/Standard: *ABAQUS, Version 5.8 User's Manual,* Hibbitt, Karlsson & Sorensen, Inc., Providence, RI. 1998.
17. Y. Liu, P. Christer, P. Bengtsson, A. Leger, and J. Wigren: "Thermal Shock Testing and Finite Element Modeling of Pre-Oxidized Thermal Barrier Coatings," in *Thermal Spray 2000: Surface Engineering via Applied Research,* C.C. Berndt, ed., ASM International, Materials Park, OH, 2000, pp. 173-80.
18. *Properties and Selection: Irons, Steels, and High-Performance Alloys,* Vol. 1, *ASM Handbook,* ASM International, Materials Park, OH, 1990.
19. D. Choules and K. Kokini: "Multilayer Ceramic Coating Architecture Against Surface Thermal Fracture," in *Proceedings of the Symposium on Ceramic Coatings,* K. Kokini, ed., ASME MD- l44 (A18), ASM International, Materials Park, OH, 1993, pp. 73-86.
20. D. Zhu and R.A. Miller: "Determination of Creep Behavior of Thermal Barrier Coatings Under Laser Imposed High Thermal and Stress Gradient Conditions," *J. Mater. Res.,* 1999, *14*(1), pp. 140-61.
21. D. Choules, K. Kokini, and T. Taylor: "Thermal Fracture of Ceramic Thermal Barrier Coatings Under High Heat Flux With Time-Dependent Behavior: Part 1. Experimental Results," *Mater. Sci. Eng.,* 2001, *A299,* pp. 296-304.
22. J.H. Hutching and A.G. Evens: "On the Delamination of Thermal Barrier Coatings in a Thermal Gradient," *Surf. Coat. Technol.,* 2002, *149,* pp. 179-84.